Science of the Total Environment 881 (2023) 163442

Contents lists available at ScienceDirect

Science of the Total Environment

journal homepage: www.elsevier.com/locate/scitotenv

Characterization of water – soluble brown carbon in atmospheric fine particles over Xi'an, China: Implication of aqueous brown carbon formation from biomass burning

Yali Lei [a], Ke Zhang [a], Yeyu Lu [a], Yiming Qin [b], Lijuan Li [c], Jianjun Li [c], Xiaodi Liu [a], Can Wu [a], Si Zhang [a], Yubao Chen [a], Junke Zhang [d], Fan Zhang [a], Gehui Wang [a,e,*]

[a] Key Lab of Geographic Information Science of the Ministry of Education, School of Geographic Sciences, East China Normal University, Shanghai 200241, China
[b] Department of Chemistry, University of California, Irvine, CA 92697 – 2025, USA
[c] State Key Laboratory of Loess and Quaternary Geology, Institute of Earth Environment, Chinese Academy of Sciences, Xi'an 710061, China
[d] Faculty of Geosciences and Environmental Engineering, Southwest Jiaotong University, Chengdu 611756, China
[e] Institute of Eco – Chongming, East China Normal University, Shanghai 202162, China

HIGHLIGHTS

- High-time resolution characterization of BrC were investigated in a heavily polluted city.
- N-containing compounds are the effective BrC chromophores.
- BBOA dominated the b_{abs365}, followed by OOA and CCOA.
- BBOA can be oxidized to produce BrC in aqueous phase.

GRAPHICAL ABSTRACT

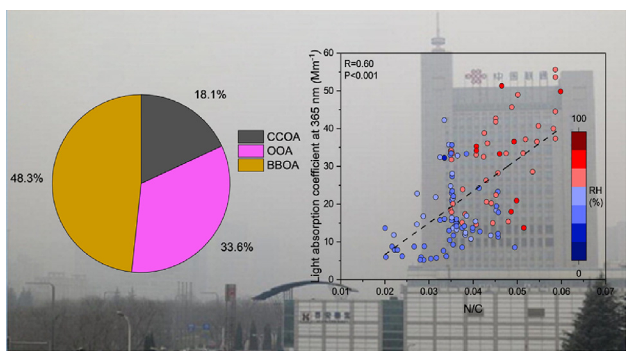

ARTICLE INFO

Editor: Jianmin Chen

Keywords:
Brown carbon
Light absorption
Sources
Aqueous formation
Xi'an

ABSTRACT

Brown carbon (BrC) aerosols can affect not only the climate but also human health, however, the light absorption, chemical compositions, and formation mechanisms of BrC are still uncertain, which leads to uncertainties in the accurate estimation of its climate and health impacts. In this study, highly time – resolved brown carbon (BrC) in fine particles was investigated in Xi'an using offline aerosol mass spectrometer analysis. The light absorption coefficient (b_{abs365}) and mass absorption efficiency (MAE_{365}) at 365 nm of water – soluble organic aerosol (WSOA) generally increased with oxygen – to – carbon (O/C) ratios, indicating that oxidized OA could have more impacts on BrC light absorption. Meanwhile, the light absorption appeared to increase generally with the increases of nitrogen – to – carbon (N/C) ratios and water – soluble organic nitrogen; strong correlations (R of 0.76 for $C_xH_yN_p^+$ and R of 0.78 for $C_xH_yO_zN_p^+$) between b_{abs365} and the N – containing organic ion families were observed, suggesting that the N – containing compounds are the effective BrC chromophores. b_{abs365} correlated relatively well with BBOA (r of 0.74) and OOA (R of 0.57), but weakly correlated with CCOA (R of 0.33), indicating that BrC in Xi'an was likely to be associated with biomass burning and secondary sources. A multiple linear regression model was applied to apportion b_{abs365} to contributions of different factors resolved from positive matrix factorization on water-soluble organic aerosols (OA) and obtained MAE_{365} values of different OA factors. We found that biomass-burning organic aerosol (BBOA) dominated the b_{abs365} (48.3 %), followed by oxidized organic aerosol (OOA, 33.6 %) and coal combustion organic aerosol (CCOA, 18.1 %). We further observed that nitrogen – containing organic matter (i.e., $C_xH_yN_p^+$ and $C_xH_yO_zN_p^+$)

* Corresponding author at: Key Lab of Geographic Information Science of the Ministry of Education, School of Geographic Sciences, East China Normal University, Shanghai 200241, China.
E-mail address: ghwang@geo.ecnu.edu.cn (G. Wang).

http://dx.doi.org/10.1016/j.scitotenv.2023.163442
Received 2 February 2023; Received in revised form 3 April 2023; Accepted 7 April 2023
Available online 12 April 2023
0048-9697/

increased with the increase of OOA/WSOA and the decrease of BBOA/WSOA, especially under high ALWC conditions. Our work offered proper observation evidence that BBOA is oxidized through the aqueous formation to produce BrC in Xi'an, China.

1. Introduction

Light − absorbing organic aerosol, or brown carbon (BrC), can significantly affect visibility, climate, and even human health (Ervens et al., 2005; Hecobian et al., 2010; Sun et al., 2011). For example, BrC might alter the hygroscopicity of atmospheric particles and their ability to act as cloud condensation nuclei (Twohy et al., 2005). BrC is also proved to act as surface active reagents, which increase the solubility of hydrophobic organic compounds, such as n − alkanes and polycyclic aromatic hydrocarbons (PAHs), and thus increase their toxicity to human health (Lei et al., 2022; Wang et al., 2003). However, the light absorption, chemical compositions, and formation mechanisms of BrC are still uncertain, hindering accurate estimations of its climate and health effects.

BrC can be emitted from primary emission (e.g., biomass burning, and coal combustion (Du et al., 2022; Lei et al., 2018a; Lei et al., 2019; Li et al., 2023; Ye et al., 2017). Meanwhile, the oxidation of volatile organic compounds (VOCs) was also proved to be a source of BrC (Laskin et al., 2015; Li et al., 2020a; Li et al., 2021a; Wu et al., 2020; Zhang et al., 2015). BrC can be formed from gas − phase photooxidation of VOCs, including biogenic VOCs and aromatic VOCs (Hu et al., 2017; Lambe et al., 2013; Laskin et al., 2015; Lee et al., 2014). In specific, aqueous in − cloud processing and oligomerization of water − soluble organics have been recognized as an important component of BrC (Gao and Zhang, 2018; Graber and Rudich, 2006; Herrmann et al., 2015; Kasthuriarachchi et al., 2020; Rodriguez et al., 2022). For example, aqueous reactions involving surface − active species may play an important role in secondary BrC formations (Rodriguez et al., 2022). Another lab study suggests that the acceleration of BrC production might be affected by the evaporation of water (Kasthuriarachchi et al., 2020). However, most aqueous BrC formations were observed in lab studies, and the field observation evidence for aqueous formations is far from conclusive.

Previous studies have illustrated that the worldwide use of Aerodyne Aerosol Mass Spectrometer (AMS) has significantly improved the chemical characterization and source apportionment of OA. However, due to the high cost and strict requirement of AMS measurement, long − term online deployments of AMS at multiple sampling sites simultaneously were restricted (Bozzetti et al., 2017). Thus, the offline AMS technique was developed to characterize the chemical characterization and sources of ambient filter samples (Chen et al., 2020; Du et al., 2022; Ge et al., 2017; Qiu et al., 2019; Ye et al., 2017), cloud/fog water (Kim et al., 2019), and aqueous − phase samples (Lu et al., 2019). Sun et al. (2011) performed the first AMS analysis of water extracts of $PM_{2.5}$ and investigated the sources of water − soluble OA (WSOA) in the southeastern U.S. via positive matrix factorization (PMF) analysis of the WSOA AMS mass spectra. Qiu et al. (2019) explored the vertical differences in the chemical characteristics and water solubility of different OA factors by performing offline AMS analysis. Moreover, this offline AMS method, together with optical analytical techniques, was also applied to investigate the chemical characterization and sources of BrC (Chen et al., 2018; Moschos et al., 2018). However, up to date, previous studies usually provide daily variations of BrC without tracking the diurnal changes of aerosol behaviors, which has brought large uncertainties to evaluate the secondary BrC absorptivity through different aging pathways. Some recent studies have utilized the AMS and multi − wavelength aethalometer to investigate the interplay among optical properties, chemical composition, and sources of BrC (de Sá et al., 2019; Qin et al., 2018). However, the inlet particle sizes of these two instruments are different. The light absorption of BrC was found to be predominately in the accumulation mode with an aerodynamic mean diameter of ~0.5 μm, which is mainly due to the chemical chromophores (Liu et al., 2013; Lei et al., 2018a). Therefore, our offline AMS measurements with high time resolution $PM_{2.5}$ collection offer a deeper insight into the understanding of BrC, especially the formation mechanisms of BrC.

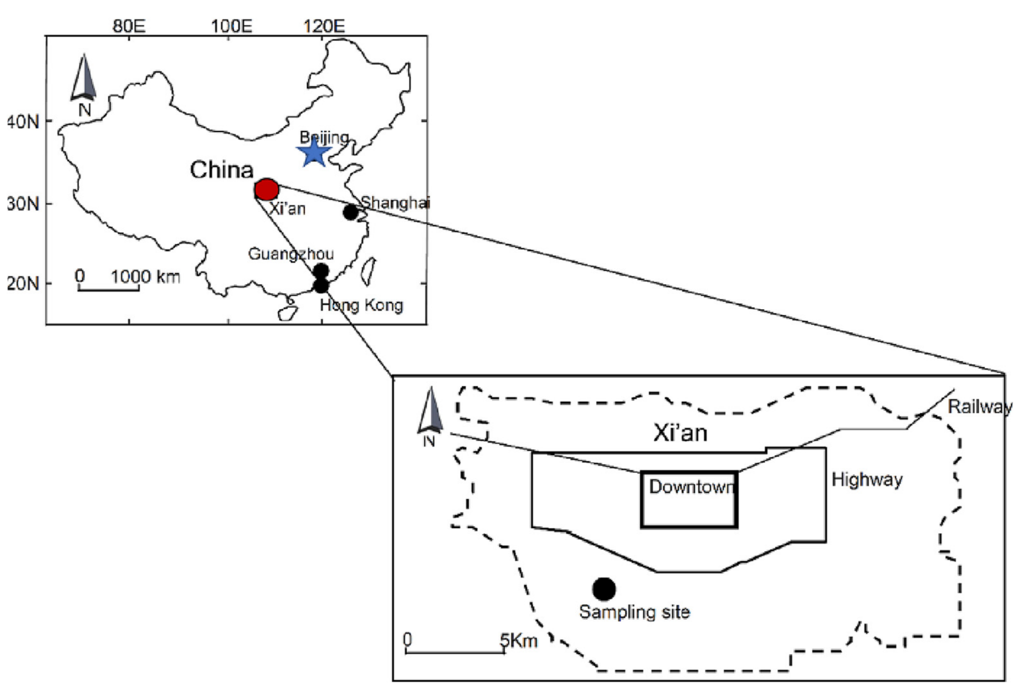

Fig. 1. Location of the sampling site (34°13′44″N, 108°53′15″E) at Xi'an, China. Sampling was conducted on the rooftop (10 m above the ground) of a three − story building at the Institute of Earth Environment, Chinese Academy of Science.

In this study, we utilized AMS to analyze water − soluble BrC in one-hour high-resolution $PM_{2.5}$ collected during wintertime in Xi'an, China, a typical city in the northwest region, representative of relatively serious air pollution in China (Huang et al., 2014; Lei et al., 2018a; Li et al., 2020a; Li et al., 2020b; Wang et al., 2016a; Wu et al., 2020; Xu et al., 2021), and other chemical species, such as water-soluble ions, PAHs, dicarboxylic acid, were also analyzed to support our results and discussion. Our highly time − resolved measurements aim to obtain a better understanding of the chemical characteristics, optical properties, sources of BrC, and in particular the formations of secondary BrC.

2. Methodology

2.1. Sample collection

The sampling site was located on the rooftop (10 m above the ground) of a three − story building on the campus of the Institute of Earth Environment, Chinese Academy of Sciences, Xi'an city, China (Fig. 1). The high − time resolution sampling was conducted from Dec. 4th to 9th, 2012 by alternately using two high volume (1.0 m^3 min^{-1}) samplers (Tianhong Instrument Co., Ltd., Wuhan, China) with one hour in each. The two samplers were calibrated before the sampling. A total of 120 samples were collected onto pre − baked (450 °C, 6–8 h) quartz fiber filters. After sampling, the filter samples were individually sealed in aluminum foil bags and stored in a freezer (−20 °C) before analysis. More details can be found in our previous study (Li et al., 2016). Meteorological parameters, including temperature and RH, were monitored by an automatic weather station (MILOS520, Vaisala, Inc., Finland), which was fixed on the roof of the observation station.

2.2. UV − Vis light absorption analyses

Water extracts of each filter sample were prepared for the UV − vis measurements. The light absorption spectra of the liquid extracts were measured over the wavelength range 190–700 nm using a UV − Vis spectrophotometer (UV − 6100 s) with 1 cm optical paths in the individual solvent. One-quarter of each filter was extracted in 25 mL Milli − Q water (18.2 MΩ) by 30 min of sonication. All extracts were filtered 1–3 times with a 25 mm diameter 0.45 μm pore size (PTFE membrane) to remove the insoluble components.

Absorption spectra of water − soluble organic carbon (WSOC) have been used to assess the b_{abs} as described by Srinivas and Sarin (2014). The b_{abs} was calculated according to:

$$b_{abs\lambda} = (A_\lambda - A_{700}) \times (V_{ext}{}^{*}\ \text{Portions}) \times \ln(10)/(V_{aero} \times L) \quad (1)$$

where $b_{abs\lambda}$ is expressed in the unit of Mm^{-1} (or 10^{-6} m^{-1}). A_λ and A_{700} correspond to measured absorbance at specified λ and 700 nm, respectively. V_{ext} refers to the volume of the solvent extract (25 mL) in which different portions of the filter. V_{aero} corresponds to the sampling volume and *L* is the path length of the cell (1 cm). "Portions" is used to estimate the absorption signal of the whole aerosol filter. For example, "Portions" shows 8 which means 1/8 portions of the aerosol filter were extracted. We have used light absorbance at 365 nm to estimate BrC b_{abs} (Liu et al., 2013).

The relationship between wavelength − dependent AAE and b_{abs} in the WSOC is described following (Hecobian et al., 2010):

$$b_{abs\lambda} = K \times \lambda^{-AAE} \quad (2)$$

Here K refers to a constant value and λ denotes the wavelength of WSOC. In this study, AAE is calculated by a linear regression fit to log b_{abs} vs. log λ in the wavelength range of 330–400 nm.

From $b_{abs\lambda}$, the mass absorption efficiency of the solubilized OA faction (MAE in m^2 g^{-1}C) can be quantified as Eq. (3). MAE of WSOC at 365 nm (MAE_{365}) was calculated based on the equation as follows:

$$MAE_\lambda = b_{abs\lambda}/WSOC \quad (3)$$

2.3. Offline AMS analysis and determination of water − soluble components

46.158 cm^2 of each filter sample was sonicated in 20 mL Milli − Q water for one hour and was then filtered with 0.45 μm PTFE syringe filters. In this

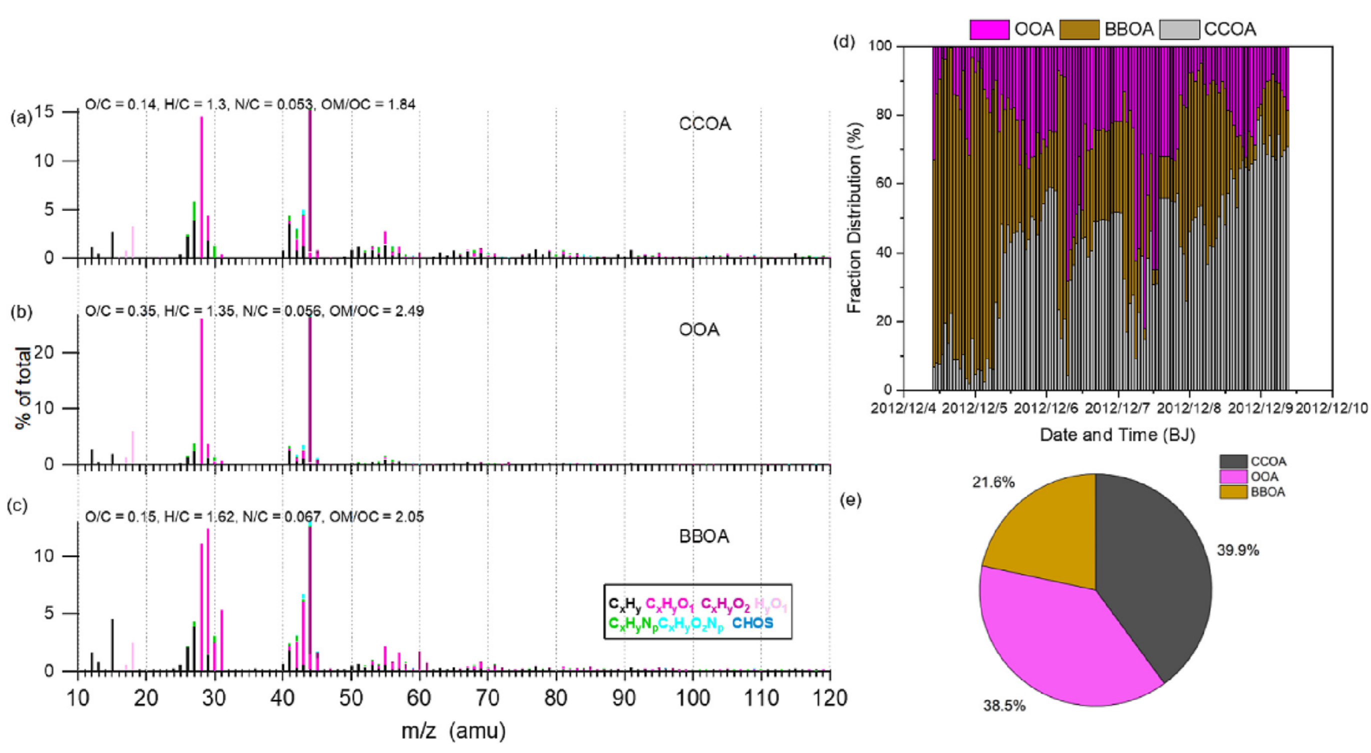

Fig. 2. (a − c) HRMS of individual water − soluble OA factors colored by different ion categories (Mass spectra of (a) CCOA; (b) OOA; (c) BBOA. Mass spectra signals are colored by six ion categories (i.e., $C_xH_y^+$, $C_xH_yO^+$, $C_xH_yO_2$, $C_3H_5O_2^+$, HO^+, $C_xH_yN^+$, and C_xH_yON); (d) time series of the mass fractional composition of WSOA; (e) the average fractional pie chart of WSOA during the study period.

study, the aerosol extractions were aerosolized by pure argon gas (Ar) using an atomizer and dehumidified via a diffusion dryer. Since we used pure argon as a carrier gas for nebulization, different from ambient measurements, CO^+, CH_2N^+, $C_2H_4^+$ ions at *m/z* 28 can be well separated and quantified from N_2^+ ions. A Milli−Q water sample was nebulized and analyzed in the same way to reduce carry−over effects. The blank samples were also analyzed using the same procedures as the filter samples. Details on AMS analysis of liquid samples are given in Chen et al. (2020) and Sun et al. (2011).

The AMS data processing was conducted using standard AMS data analysis software SQUIRREL v1.56 and PIKA v1.15 written in Igor Pro (Wavemetrics, Lake Oswego, OR, USA) (Chen et al., 2020). Elemental analysis was conducted on the ion−speciated HRMS to determine the atomic oxygen−to−carbon (O/C), hydrogen−to−carbon (H/C), nitrogen−to−carbon (N/C), and organic mass − to−carbon (OM/OC) ratios following the Improved−Ambient (IA) method (Canagaratna et al., 2015).

To convert the chemical species concentration in the nebulized aerosol to those in the ambient air, the sulfate signal was used as an internal standard. Since sulfate is nonvolatile and water−soluble, we assume it was extracted at 100 % efficiency by water. We also assume that the fractional composition sampled by ion chromatography (Dionex 600, Dionex, US) and filter samples is the same. Thus, the concentration of organic matter measured by the AMS in the nebulized aerosol ($[Org]_{AMS}$) can be converted to ambient concentration (WSOA) by applying the ratio between the sulfate concentration measured in filter extract by the AMS ($[SO_4^{2-}]_{AMS}$) and the average ambient sulfate concentration measured by IC over the corresponding period ($[SO_4^{2-}]_{ambient}$):

$$\mathrm{WSOA} = [\mathrm{Org}]_{\mathrm{AMS}} \times \left([\mathrm{SO_4}^{2-}]_{\mathrm{ambient}} / [\mathrm{SO_4}^{2-}]_{\mathrm{AMS}} \right) \tag{4}$$

Three factors including coal combustion OA (CCOA), biomass burning OA (BBOA), and oxidized oxygenated OA (OOA) were resolved using positive matrix factorization (PMF).

2.4. Other chemical analysis

The water−soluble organic carbon (WSOC), organic carbon (OC), water-soluble inorganic ions, polycyclic aromatic hydrocarbons (PAHs), and dicarboxylic acid analyses were described in our previous studies (Li et al., 2016). Briefly, the WSOC concentrations were quantified by a TOC analyzer (TOC − L CPH, Shimadzu, Japan) (Li et al., 2016; Shen et al., 2017; Wang et al., 2018a). The concentrations of OC were measured by the OC/EC analyzer (DRI, 2001A, USA) following the Interagency Monitoring of Protected Visual Environments (IMPROVE) thermal/optical reflectance (TOR) protocol (Lei et al., 2019; Li et al., 2016). Water−soluble inorganic ions were analyzed by using ion chromatography (Dionex 600, Dionex, USA) (Li et al., 2016). The organic compounds including PAHs and dicarboxylic acid were determined using gas chromatography/mass

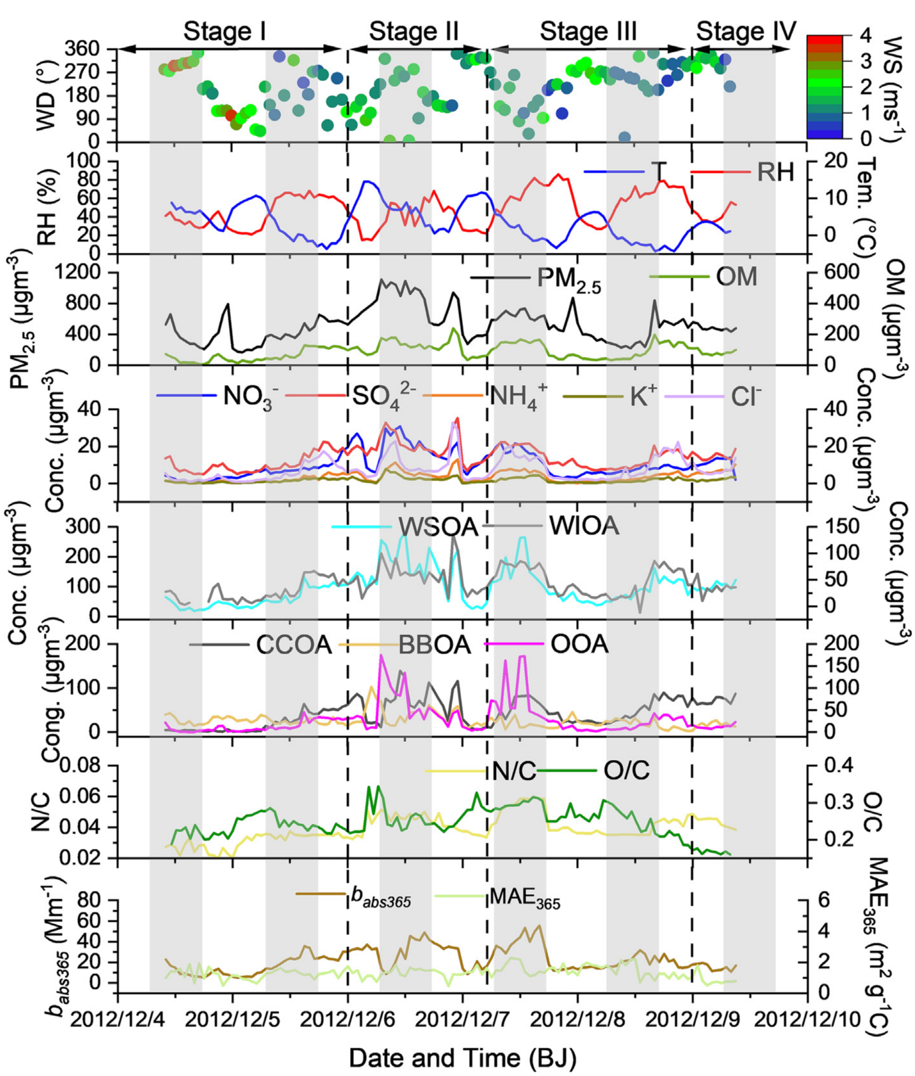

Fig. 3. Time series of meteorological parameters, chemical species and light absorption parameters measured in Xi'an on Dec. 4–9, 2012.

spectrometry (GC/MS). GC/MS analysis of the derivatives was performed using an Agilent 7890A GC coupled with an Agilent 5975C MSD. The GC separation was carried out using a DB − 5MS fused silica capillary column with the GC oven temperature programmed from 50 °C (2 min) to 120 °C at 15 °C min^{-1} and then to 300 °C at 5 °C min^{-1} with a final isothermal hold at 300 °C for 16 min. The sample was injected in a splitless mode at an injector temperature of 280 °C, and scanned from 50 to 650 Da using electron impact (EI) mode at 70 eV. More details can be found in our previous studies (Li et al., 2022; Wang et al., 2009).

2.5. Aerosol liquid water content calculation

The measured concentrations of water − soluble inorganic ions and daily averaged temperature and RH (relative humidity) were used as input in the aerosol thermodynamic model ISORROPIA − II (Fountoukis and Nenes, 2007) to calculate aerosol liquid water content and pH for particles. In this study, the forward metastable mode was chosen for the estimation since it is less sensitive to measurement errors that the reverse mode (Guo et al., 2015; Hennigan et al., 2015; Lv et al., 2022; Wu et al., 2019). By the way, organics on aerosol liquid water content and pH were not taken into account due to the small effects in China (Liu et al., 2017).

3. Results and discussion

3.1. Temporal variations of WSOA

To investigate water − soluble organic aerosols (WSOA), three WSOA factors were first identified via PMF analysis of the HRMS of WSOA, namely CCOA, BBOA, and OOA. Fig. 2 presents a summary of the mass spectral profiles, time series, and the mass fractional contributions of these three factors. On average, PMF source apportionment results showed that WSOA were composed of 39.9 % CCOA, 38.5 % OOA, and 21.6 % BBOA.

As seen in Fig. 2a, the mass spectrum of CCOA is characterized by alkyl fragments, such as $C_nH_{2n+1}^+$, $C_nH_{2n-1}^+$, and the reprehensive primary OA (POA) ions from fossil fuel combustion. Meanwhile, CCOA presents a unique peak of $C_7H_7^+$ at *m/z* 91, the spectral marker of coal combustion. The O/C and H/C ratios of CCOA are 0.14 and 1.30, respectively. In addition, good correlations were observed between CCOA and benzo(*b*)fluoranthene (BbF), benzo(*a*)pyrene (BaP), and $C_2H_4O_2^+$ (Fig. S1), which are proved to be coal combustion tracers observed in our study (Lei et al., 2021; Qiu et al., 2019; Wang et al., 2021). The mass spectrum of OOA is characterized by a prominent peak of *m/z* 44 (mainly CO_2^+) (Fig. 2b). Meanwhile, the O/C and OM/OC ratios were 0.35 and 2.49. Moreover, we also noticed a relatively good relationship between OOA and oxalic acid, an SOA tracer (Fig. S2). Biomass burning is a significant WSOA source because primary BBOA consists of water − soluble species, i.e., anhydrous sugar (Ge et al., 2017). The mass spectrum of BBOA is contributed by $C_xH_y^+$ and $C_xH_yO_z^+$ ions. In specific, BBOA is characterized by prominent peaks at *m/z* 60 ($C_2H_4O_2^+$), the typical ion fragments of anhydrous sugars (e.g., levoglucosan) (Cubison et al., 2011). Another evidence was that BBOA is closely correlated with those of levoglucosan (R = 0.83, Fig. S3b) and K^+ (R = 0.82, Fig. S3c).

The temporal variation of WSOA and meteorological parameters in this study were illustrated in Fig. 3. Winds were weak throughout the sampling period, indicative of stagnant conditions. The period of December 4–6, denoted as Stage I in Fig. 3, was characterized by moderate RH (47.3 ± 20.1 %) and a mean temperature of 3.7 ± 4.4 °C (Table 1). The period of December 6–7, denoted as Stage II, had a lower RH (37.4 ± 14.9 %) and a higher temperature (7.8 ± 4.1 °C). Additionally, the period from December 7 to 9, denoted as Stage III with higher RH (60.5 ± 17.0 %) and lowest temperature (0.3 ± 3.3 °C). A pronounced increase of OOA mass concentration during Stage III with higher RH further supports the formation of OOA through aqueous − phase chemistry. Previous AMS field studies in China have identified OOA, an important OA component, can be produced in the aqueous phase under high − RH conditions (Wang et al., 2021).

Table 1
Mass concentrations of $PM_{2.5}$ and its chemical species in four stages.

Species	Stage I		Stage II		Stage III		Stage IV	
	Mean	SD[a]	Mean	SD[a]	Mean	SD[a]	Mean	SD[a]
$PM_{2.5}$ (μgm^{-3})	254.3	128.1	573.2	247.4	355.5	165.0	329.9	30.2
Wind speed (ms^{-1})	1.8	0.9	1.5	0.4	1.3	0.5	1.3	0.7
T (°C)	3.7	4.4	7.8	4.1	0.3	3.3	2.5	1.1
RH (%)	47.3	20.1	37.4	14.9	60.5	17.0	42.2	8.1
CCOA (μgm^{-3})	19.4	21.3	57.4	39.3	49.4	24.1	71.4	8.9
OOA (μgm^{-3})	12.8	12.4	46.6	43.9	33.1	41.6	12.3	4.5
BBOA (μgm^{-3})	25.6	7.7	36.7	22.6	18.4	10.3	18.0	5.0
WSOA (μgm^{-3})	57.8	31.5	140.7	73.9	101.0	53.3	101.7	13.2
WSOC (μgm^{-3})	15.2	9.9	29.5	16.8	25.1	22.3	23.3	6.8
TC (μgm^{-3})	45.8	31.8	88.9	40.5	78.8	42.4	66.5	12.1
OC (μgm^{-3})	35.4	24.8	71.3	30.3	59.6	32.1	49.9	9.6
EC (μgm^{-3})	10.4	7.3	17.6	10.6	19.2	10.5	16.6	3.0
OC/EC	3.6	1.1	4.4	0.9	3.1	0.3	3.0	0.3
NO_3^- (μgm^{-3})	5.9	4.3	17.4	7.6	9.4	5.5	11.1	3.7
SO_4^{2-} (μgm^{-3})	10.7	5.1	19.2	6.9	13.8	5.1	14.7	2.0
Na^+ (μgm^{-3})	2.3	1.3	5.0	1.6	2.6	1.4	4.3	1.1
NH_4^+ (μgm^{-3})	1.8	1.7	4.7	3.3	3.6	2.5	6.8	1.5
K^+ (μgm^{-3})	1.2	0.9	2.5	1.9	1.8	1.3	2.2	0.8
Levoglucosan (μgm^{-3})	0.5	0.5	1.0	0.7	1.1	1.4	0.5	0.2
Phenanthrene (ngm^{-3})	12.6	13.3	21.8	11.8	28.6	22.3	24.9	5.6
Anthracene (ngm^{-3})	1.0	1.1	1.4	0.9	2.8	2.2	3.4	1.1
Fluoranthene (ngm^{-3})	16.6	19.8	24.5	15.8	31.7	21.5	34.9	7.7
Pyrene (ngm^{-3})	14.4	18.6	22.2	16.4	28.8	22.8	24.7	7.7
Benz(*a*)anthracene (ngm^{-3})	6.6	9.4	9.8	8.7	12.7	11.8	7.5	3.4
Chrysene (ngm^{-3})	9.8	12.5	15.4	11.3	17.3	13.1	14.9	4.2
benzo(*b*)fluoranthene (ngm^{-3})	10.9	13.5	18.0	13.5	20.3	17.0	15.8	4.4
benzo(*k*)fluoranthene (ngm^{-3})	2.9	3.6	5.2	4.0	6.1	5.1	5.1	1.3
benzo(*e*)pyrene (ngm^{-3})	7.0	9.1	10.9	8.1	12.9	10.5	10.0	2.8
benzo(*a*)pyrene (ngm^{-3})	6.3	8.8	10.4	9.0	13.3	12.6	8.4	3.3
Perylene (ngm^{-3})	1.5	2.1	2.5	2.1	3.1	3.0	1.6	0.7
Indeno[123-*cd*]pyrene (ngm^{-3})	6.2	7.7	10.2	8.0	12.1	10.9	9.1	2.6
Dibenz(*a,h*)anthracene (ngm^{-3})	1.4	1.6	1.7	1.2	2.1	1.7	1.6	0.5
Benzo(*ghi*)perylene (ngm^{-3})	6.4	7.8	10.1	7.7	12.1	10.7	8.7	2.2
Coronene (ngm^{-3})	2.1	2.7	3.4	3.0	4.1	4.1	2.6	0.8
Dibenzo(*a,e*)pyrene (ngm^{-3})	0.6	0.8	0.7	0.6	1.1	1.0	0.7	0.2
Total PAHs (ngm^{-3})	109.2	134.2	168.3	120.4	212.0	168.1	173.7	46.4
Oxalic acid (μgm^{-3})	0.3	0.1	0.6	0.2	0.3	0.1	0.3	0.0

[a] Standard deviation.

3.2. Light absorption of WSOA

Fig. 4a illustrates the light absorption spectra of water − soluble extracts from 300 to 700 nm. As can be seen in Fig. 4a, the light absorption of water − soluble extracts decreased dramatically from 300 nm to 700 nm. In specific, the absorption at the wavelength of 365 nm has been widely used to represent the light absorptivity of BrC (Lei et al., 2018a), which is chosen to avoid the interferences by inorganic compounds (e.g., nitrate). High correlation of b_{abs365} with WSOA (R = 0.86, Fig. 4b) was found in this study, suggesting that WSOA contains a significant portion of BrC chromophores. As shown in Fig. 4c − d, b_{abs365} presented good correlations with two biomarkers (R of 0.68 and 0.71 for K^+ and Levoglucosan, respectively), indicating that biomass burning emissions might be important BrC sources in this study. Meanwhile, good correlations between b_{abs365} and BaP (R = 0.61) and BbF (R = 0.62) were also observed, inferring that coal combustion can be an important source of BrC. Furthermore, b_{abs365} also correlated with oxalic acid, suggesting secondary formation to some extent contributed to BrC. Moreover, b_{abs365} presented good correlations with EC (R =

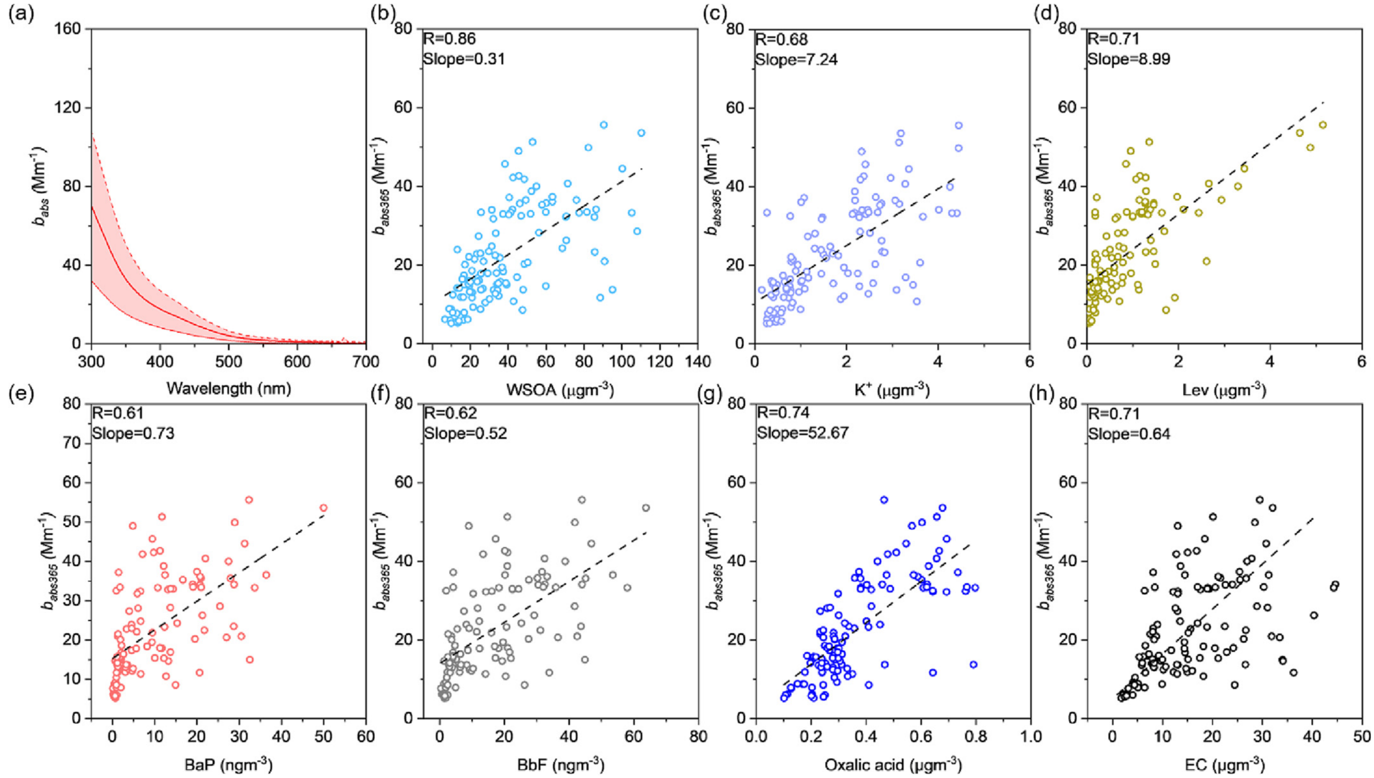

Fig. 4. (a) Averaged light absorption spectra of water extracts, scatter plots of light absorption coefficient at 365 nm of WSOA versus (b) WSOA, (c) K^+, (d) Levoglucosan (Lev), (e) BaP, (f) BbF, (g) Oxalic acid, and (h) EC.

0.71), demonstrating that combustion emissions may be important BrC sources in this study.

The temporal variations of b_{abs365} and MAE_{365} were displayed in Fig. 3. The average b_{abs365} during the sampling period was 22.6 ± 12.3 Mm^{-1}, which is similar to the previous studies observed in Xi'an (Shen et al., 2017), but much higher than those obtained in Seoul, Korea (3.76 Mm^{-1}; Kim et al. (2016)), southeastern US in summer (0.21 Mm^{-1}; Xie et al. (2019)), Beijing, China during wintertime (10.48 Mm^{-1}; Cheng et al. (2016)). A new study written by Wang et al. (2022) found that the b_{abs365} values for BrC exhibited significant spatial variations across these six cities in China (Beijing, Harbin, Xi'an, Chengdu, Guangzhou, and Wuhan). The MAE_{365} was 1.31 ± 0.40 $m^2\ g^{-1}C$, which is in agreement with earlier studies (Chen et al., 2020; Cheng et al., 2016; Du et al., 2014; Kim et al., 2016; Lei et al., 2019). Therefore, the differing results observed in different areas implied that the light absorption of BrC could be influenced by chemical structures (Zeng et al., 2021; Zhang et al., 2020), atmospheric aging (Al-Abadleh, 2021; Li et al., 2021a; Rodriguez et al., 2022).

In addition, the diurnal variation of b_{abs365} and MAE_{365} are depicted in Fig. S4. On the whole, b_{abs365} and MAE_{365} presented relatively high levels in the nighttime but low concentrations during the daytime. Our results suggest diurnal characteristics of aerosol optical properties during the heating season in north China, that is, the increased light absorption during nighttime due to enhanced aqueous production of secondary aerosol (Gilardoni et al., 2016). In addition, the decrease in b_{abs365} in the afternoon may be related to the photobleaching of BrC due to intense photochemical processes (Du et al., 2022; Lei et al., 2019).

3.3. Chemical properties of water − soluble BrC

In this study, the variations of b_{abs365} together with atomic oxygen to carbon (O/C) ratios were illustrated in Fig. 5a. The b_{abs365} values generally increased with O/C ratios. Similar results were found for MAE_{365} versus O/C ratios in Fig. 5b. This observation again indicates that oxidized OA could have more impacts on BrC light absorption (Jiang et al., 2022). However, the enhanced formation of BrC is not well in agreement with earlier photo − bleaching observations in wintertime Nanjing, China (Chen et al., 2018) or dry seasons in central Amazonia (de Sá et al., 2019). Laboratory investigations showed that chemical aging can significantly affect the light absorptivity of atmospheric BrC, but both photobleaching and photo − enhancement are possible owing to different precursors or aging conditions (for example, reaction time) (Choudhary et al., 2023; Di Lorenzo and Young, 2016; Wong et al., 2017; Yu et al., 2014). Previous studies found that the photo-enhancement in BrC absorbance during aqueous oxidation (Wong et al., 2019; Hems et al., 2020). The observed results that b_{abs365} increases with the increase of O/C may reflect some local characteristics of BrC, which may also be related to the subsequent claim of secondary BrC generation by the liquid-phase reaction of BBOA. For example, as relatively high humidity can provide an aqueous phase medium, Maillard reaction is supposed to occur during our sampling period (Chen et al., 2021a, 2021b). Meanwhile, it has been suggested that nitrocatechols, which are formed through atmospheric oxidation of biomass burning, are the major contributors to atmospheric BrC (Frka et al., 2016). Moreover, another study have found that nitrophenols are observed to contribute to the light absorption in BrC aerosol from biomass burning, and they are reactive toward oxidation, especially in the aqueous phase (Hems and Abbatt, 2018). b_{abs365} and MAE_{365} versus nitrogen − to − carbon (N/C) ratios and water − soluble organic nitrogen ions concentrations were also investigated in Figs. 5 c − d and 6a − b. It can be seen that both b_{abs365} and MAE_{365} increased with the increase of N/C ratios and water − soluble organic nitrogen ions concentrations. Moreover, high correlations for $C_xH_yN_p^+$ (R = 0.76) and $C_xH_yO_zN_p^+$ (R = 0.78) were observed between b_{abs365} in the AMS measurements, highlighting the N − containing compounds were significant BrC chromophores (Chen et al., 2017; Chen et al., 2019a; Chen et al., 2019b).

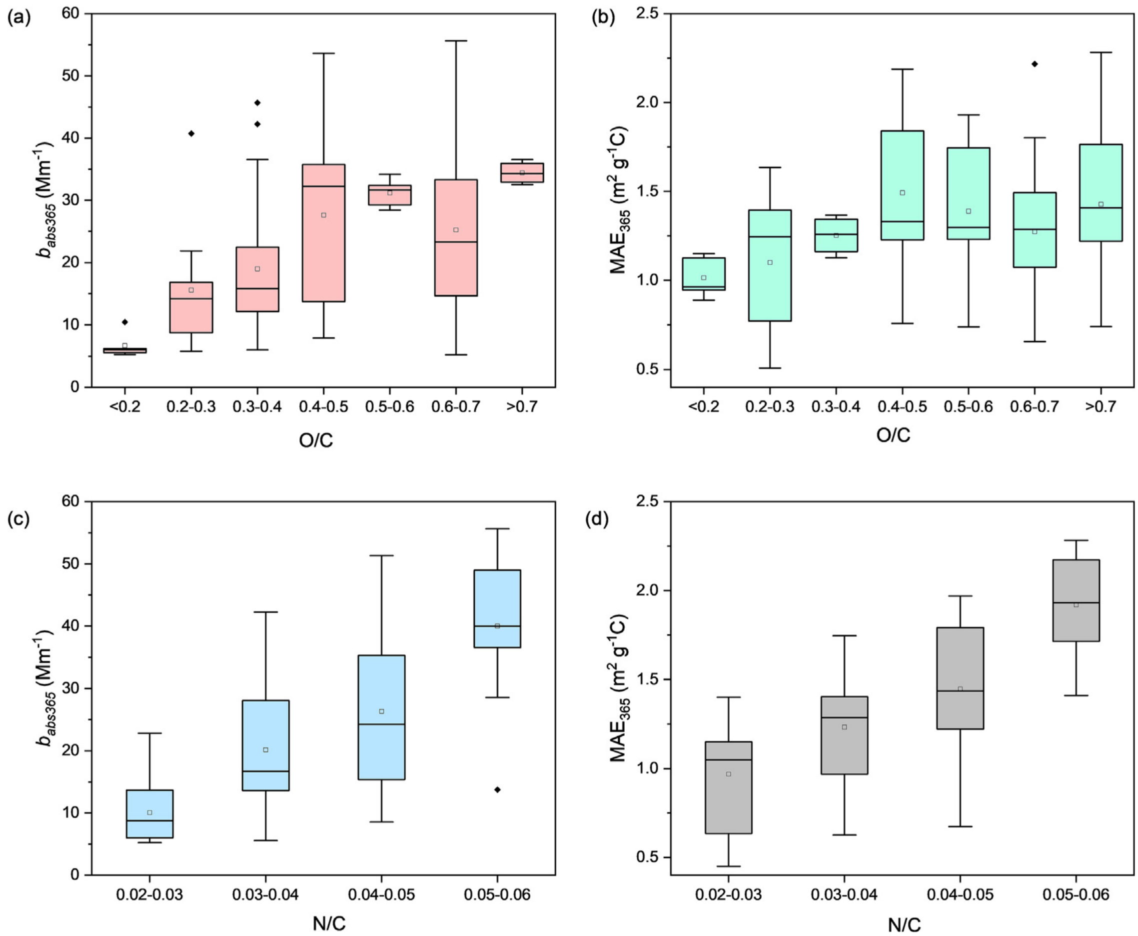

Fig. 5. Box plot of (a) b_{abs365} versus O/C, (b) MAE_{365} versus O/C, (c) b_{abs365} versus N/C, and (d) MAE_{365} versus N/C.

3.4. b_{abs365} source apportionment

To explore the three water – soluble factors to BrC, the correlations between b_{abs365} and these factors were first investigated. As seen in Fig. S5, b_{abs365} correlated relatively well with BBOA (r of 0.74) and OOA (R of 0.57), but weakly correlated with CCOA (R of 0.33), indicating that BrC in Xi'an was likely to be associated with biomass burning and secondary sources. These results are found to be consistent with a recent study in Yangzhou, China (Chen et al., 2020). Moreover, the mass spectra of BBOA and OOA have relatively high N/C ratios (0.067 for BBOA, 0.056 for OOA) and high N − containing organic ions fractions ($C_xH_yN_p^+$: 18.2 % for BBOA and 11.8 % for OOA, and $C_xH_yO_zN_p^+$).

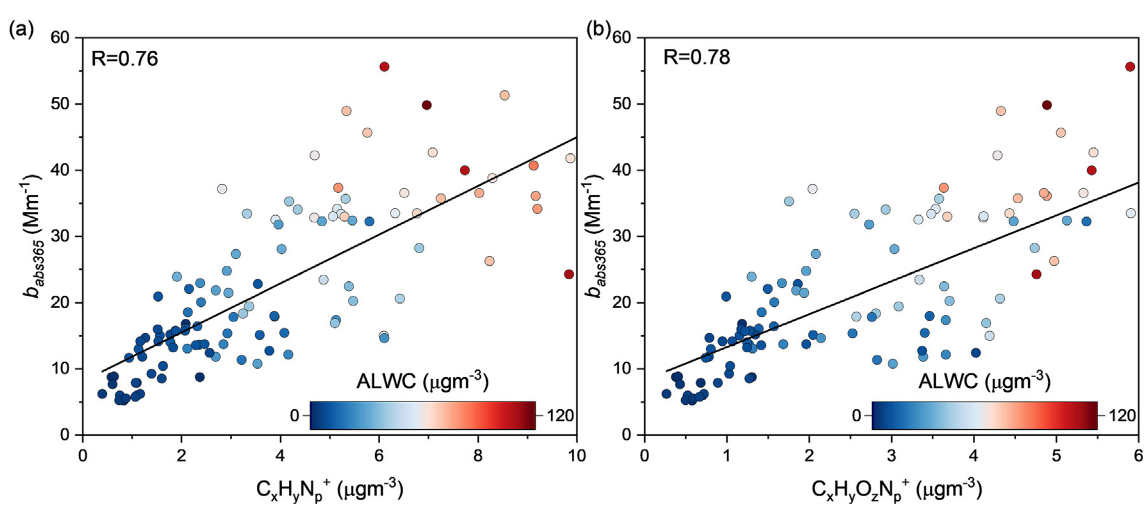

Fig. 6. Correlations between b_{abs365} and mass concentrations of N − containing organic ion families with the changing ALWC.

Table 2
Summary of the multiple linear regression results based on (a) three WSOA factors and (b) three WSOM factors.

	Coefficients ($m^2 g^{-1} C$)		Contributions (%)
	Mean	SD[a]	
CCOA	0.41	0.06	18.1
BBOA	0.68	0.08	48.3
OOA	0.48	0.04	33.6

[a] Standard deviation.

We then used multiple linear regression (MLR) algorithms (Lei et al., 2018b) to apportion the contributions of different WSOA factors to the b_{abs365} via the following equation:

$$b_{abs365} = a[\mathrm{CCOA}] + b[\mathrm{OOA}] + c[\mathrm{BBOA}] \quad (5)$$

where [CCOA], [OOA], and [BBOA] are time series of WSOA factors, and a, b, and c are the regression coefficients (Table 2), which are the MAE values ($m^2 g^{-1}C$) of corresponding factors. The correlation coefficient between reconstructed b_{abs365} and was 0.91 with a slope of 0.93 (Fig. S6a), suggesting the effectiveness of this algorithm on this dataset. Fig. 8b displayed the source contributions of different WSOA factors to b_{abs365}. It can be seen that BBOA dominated the b_{abs365} (48.3 %), followed by OOA (33.6 %) and CCOA (18.1 %). Therefore, OOA also contributed to BrC absorptivity besides BBOA. This is possibly due to the aging processing with the compounds having a relatively higher BrC chromophore such as humic − like substances (HULIS). HULIS formation was related to aqueous processing from biomass burning (Graber and Rudich, 2006; Hecobian et al., 2010; Lin et al., 2010). Moreover, previous studies have also illustrated that the PAHs aqueous oxidation might contribute to BrC absorptivity (Haynes et al., 2019; Liu et al., 2020; Wang et al., 2021). For example, nitroaromatic compounds, the derivatives of PAHs, can produce secondary BrC through the oxidation of aromatic precursors from biomass burning emissions (Desyaterik et al., 2013).

3.5. Implications of aqueous brown carbon formation from biomass burning

As is known to all, some secondary BrC processes can cause an increase in light absorption, while others lead to bleaching (Al-Abadleh, 2021; Dasari et al., 2019; Hems and Abbatt, 2018; Hems et al., 2021; Laskin et al., 2015; Sumlin et al., 2017). Therefore, these have brought large uncertainties in the absorption intensity of different OA and how the light absorption changes through atmospheric aging in modeling (Wang et al., 2018b; Wang et al., 2016b).

It can be seen from Fig. 7a − b that BBOA/WSOA decreased with the increase of ALWC while OOA/WSOA increased with the increase of ALWC, suggesting the aqueous formation of oxidized OA from BBOA in our campaign. It can be also inferred by the Van Krevelen diagram of water − soluble OA (Fig. S7). The Van Krevelen diagram tracks the evolution of WSOA based on H/C ratios and O/C ratios. H/C decreased with O/C increased in the succession from BBOA to OOA. Meanwhile, the higher light absorption of water − soluble OA was observed with higher oxidized ions such as CO_2^+ (Fig. 7c) and oxalic acid (Fig. 7d). Moreover, nitrogen − containing organic matter (i.e., $C_xH_yN_p^+$ and $C_xH_yO_zN_p^+$) increased with the increase of OOA/WSOA and the decrease of BBOA/WSOA, especially under high ALWC conditions.

Our observations implied that the enhanced BrC formation is likely to be associated with aqSOA formation, which is consistent with the previous study investigated by Gilardoni et al. (2016). Another campaign evidence for BrC formation through aqueous processing has also been observed for fog processing of biomass burning during periods of high aerosol liquid water content in wintertime in Xianghe, China, as well (Wang et al., 2019). Furthermore, our result agrees with the measurements of optical properties of aqSOA produced in laboratory experiments from photooxidation and nitration of phenolic compounds (Kitanovski et al., 2014; Lambe et al., 2013; Yu et al., 2014). Therefore,

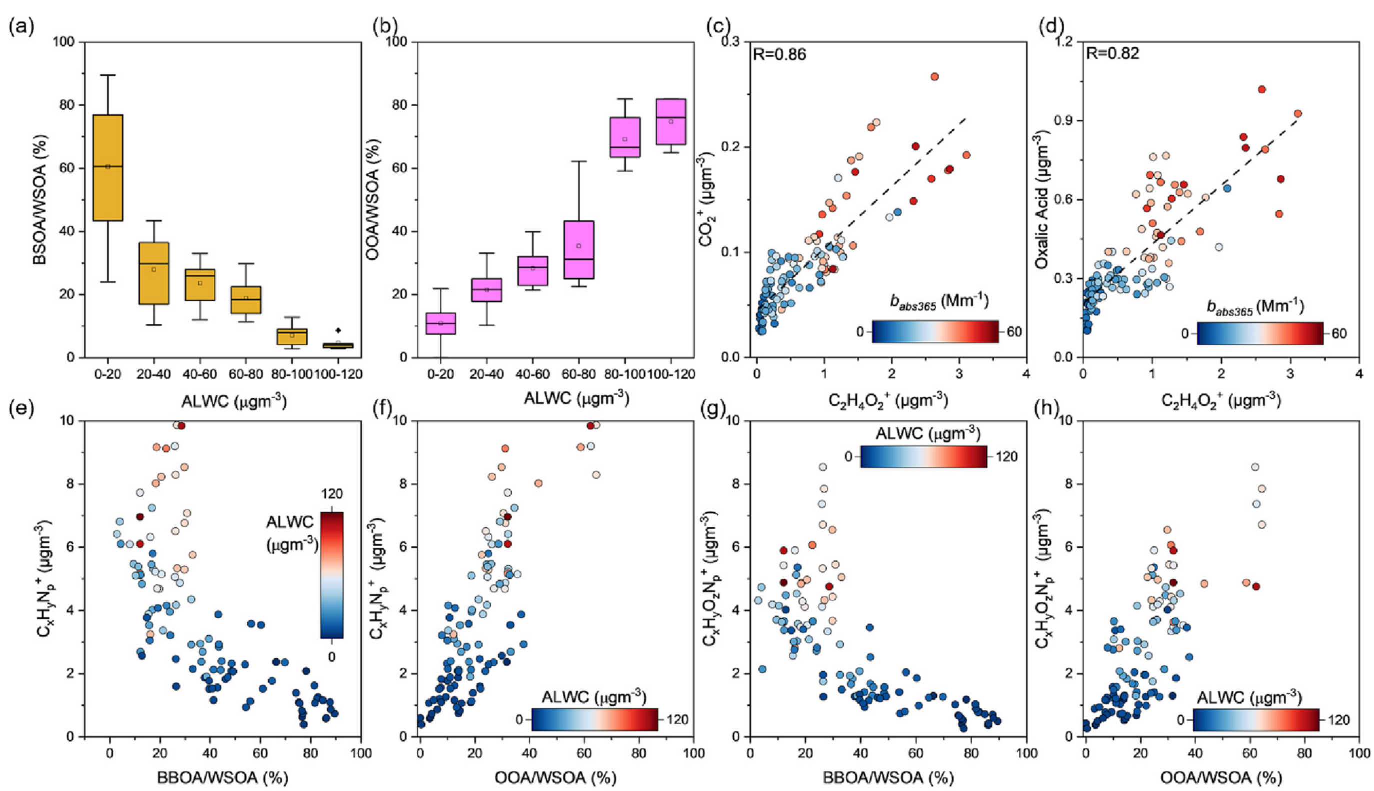

Fig. 7. Box plot of (a) BBOA/WSOA and (b) OOA/WSOA versus ALWC; Scatterplot of (c) CO_2^+ versus $C_2H_4O_2^+$, (d) Oxalic acid versus $C_2H_4O_2^+$, $C_xH_yN_p^+$ versus (e) BBOA/WSOA and (f) OOA/WSOA, $C_xH_yO_zN_p^+$ versus (g) BBOA/WSOA and (h) OOA/WSOA with the changing ALWC.

our work offered proper observation evidence that BBOA is oxidized to produce BrC in the aqueous phase in Xi'an, China.

4. Summary and conclusion

Our study investigated the light absorption properties of water − soluble BrC in $PM_{2.5}$ in Xi'an, China, a typical city in the northwest region, representative of relatively serious air pollution in China. The b_{abs365} and MAE_{365} were 22.6 ± 12.3 Mm^{-1} and 1.31 ± 0.40 m^2 $g^{-1}C$, respectively. The chemical properties of water − soluble BrC showed that both b_{abs365} and MAE_{365} values appeared to increase in general with the increases of N/C ratios and WSON concentrations. Moreover, strong correlations ($r > 0.75$) were observed between b_{abs365} and the N − containing organic ion families (i.e., $C_xH_yN_p^+$, $C_xH_yO_zN_p^+$) from AMS measurements, highlighting that the N − containing compounds are the effective BrC chromophores. The source apportionment of b_{abs365} showed that BBOA dominated the b_{abs365} (48.3 %), followed by OOA (33.6 %) and CCOA (18.1 %). Meanwhile, BBOA/WSOA decreased with the increase of ALWC while OOA/WSOA increased with the increase of ALWC. Moreover, most of the high-value plots of ALWC have higher b_{abs365} and MAE_{365}, indicating that BrC is related to the formation of the liquid phase and produces higher nitrogen − containing organic matter. However, due to the complex BrC molecules that can change the evaporation and hydration properties through aqueous reactions, understanding the physicochemical effects of BrC molecules is still needed to obtain a good grasp of the parameters in the models.

CRediT authorship contribution statement

Wang GH designed the research; Lei YL, Li JJ, Zhang K, Lu YY, and Chen YB conducted the sampling and chemical analysis; Lei YL contributed to writing the draft manuscript; Zhang K, Lu YY, Qin YM, Li LJ, Wu C, Zhang JK, Zhang F, and Wang GH were responsible for reviewing and editing the manuscript; Wang GH supervised the study.

Data availability

Data will be made available on request.

Declaration of competing interest

The authors declare that they have no known competing financial interests or personal relationships that could have appeared to influence the work reported in this paper.

Acknowledgment

This research is financially supported by the National Natural Science Foundation of China (42130704, 42107107). The authors thank Dr. Junfeng Wang at Nanjing University of Information Science & Technology for his vital contributions to AMS data analysis. We also thank all the authors for their helpful discussions and constructive comments on this work.

Appendix A. Supplementary data

Supplementary data to this article can be found online at https://doi.org/10.1016/j.scitotenv.2023.163442.

References

Al-Abadleh, H.A., 2021. Aging of atmospheric aerosols and the role of iron in catalyzing brown carbon formation. Environ. Sci.Atmos. 1, 297–345.

Bozzetti, C., Sosedova, Y., Xiao, M., Daellenbach, K.R., Ulevicius, V., Dudoitis, V., Mordas, G., Byčenkienė, S., Plauškaitė, K., Vlachou, A., Golly, B., Chazeau, B., Besombes, J.L., Baltensperger, U., Jaffrezo, J.L., Slowik, J.G., El Haddad, I., Prévôt, A.S.H., 2017. Argon offline-AMS source apportionment of organic aerosol over yearly cycles for an urban, rural, and marine site in northern Europe. Atmos. Chem. Phys. 17, 117–141.

Canagaratna, M.R., Jimenez, J.L., Kroll, J.H., Chen, Q., Kessler, S.H., Massoli, P., Hildebrandt Ruiz, L., Fortner, E., Williams, L.R., Wilson, K.R., Surratt, J.D., Donahue, N.M., Jayne, J.T., Worsnop, D.R., 2015. Elemental ratio measurements of organic compounds using aerosol mass spectrometry: characterization, improved calibration, and implications. Atmos. Chem. Phys. 15, 253–272.

Chen, Q., Ikemori, F., Nakamura, Y., Vodicka, P., Kawamura, K., Mochida, M., 2017. Structural and light-absorption characteristics of complex water-insoluble organic mixtures in urban submicrometer aerosols. Environ. Sci. Technol. 51, 8293–8303.

Chen, Y., Ge, X., Chen, H., Xie, X., Chen, Y., Wang, J., Ye, Z., Bao, M., Zhang, Y., Chen, M., 2018. Seasonal light absorption properties of water-soluble brown carbon in atmospheric fine particles in Nanjing,China. Atmos. Environ. 187, 230–240.

Chen, Q., Sun, H., Wang, M., Wang, Y., Zhang, L., Han, Y., 2019a. Environmentally persistent free radical (EPFR) formation by visible-light illumination of the organic matter in atmospheric particles. Environ. Sci. Technol. 2019 (53), 10053–10061.

Chen, Q., Sun, H., Mu, Z., Wang, Y., Li, Y., Zhang, L., Wang, M., Zhang, Z., 2019b. Characteristics of environmentally persistent free radicals in PM2.5: concentrations, species and sources in Xi'an, Northwestern China. Environ. Pollut. 247, 18–26.

Chen, Y., Xie, X., Shi, Z., Li, Y., Gai, X., Wang, J., Li, H., Wu, Y., Zhao, X., Chen, M., Ge, X., 2020. Brown carbon in atmospheric fine particles in Yangzhou, China: light absorption properties and source apportionment. Atmos. Res. 244, 105028.

Chen, Q., Hua, X., Dyussenova, A., 2021a. Evolution of the chromophore aerosols and its driving factors in summertime Xi'an, Northwest China. Chemosphere 281, 130838.

Chen, Q., Hua, X., Li, J., Chang, T., Wang, Y., 2021b. Diurnal evolutions and sources of water-soluble chromophoric aerosols over Xi'an during haze event, in Northwest China. Sci. Total Environ. 786, 147412.

Cheng, Y., He, K., Du, Z., Engling, G., Liu, J., Ma, Y., Zheng, M., Weber, R.J., 2016. The characteristics of brown carbon aerosol during winter in Beijing. Atmos. Environ. 127, 355–364.

Choudhary, V., Roson, M.L., Guo, X., Gautam, T., Gupta, T., Zhao, R., 2023. Aqueous-phase photochemical oxidation of water-soluble brown carbon aerosols arising from solid biomass fuel burning. Environ. Sci. Atmos. https://doi.org/10.1039/D2EA00151A.

Cubison, M.J., Ortega, A.M., Hayes, P.L., Farmer, D.K., Day, D., Lechner, M.J., Brune, W.H., Apel, E., Diskin, G.S., Fisher, J.A., Fuelberg, H.E., Hecobian, A., Knapp, D.J., Mikoviny, T., Riemer, D., Sachse, G.W., Sessions, W., Weber, R.J., Weinheimer, A.J., Wisthaler, A., Jimenez, J.L., 2011. Effects of aging on organic aerosol from open biomass burning smoke in aircraft and laboratory studies. Atmos. Chem. Phys. 11, 12049–12064.

Dasari, S., Andersson, A., Bikkina, S., Holmstrand, H., Budhavant, K., Satheesh, S., Asmi, E., Kesti, J., Backman, J., Salam, A., Bisht, D.S., Tiwari, S., Hameed, Z., Gustafsson, Ö., 2019. Photochemical degradation affects the light absorption of water-soluble brown carbon in the south asian outflow. Sci. Adv. 5, eaau8066.

Desyaterik, Y., Sun, Y., Shen, X., Lee, T., Wang, X., Wang, T., Collett Jr., J.L., 2013. Speciation of "brown" carbon in cloud water impacted by agricultural biomass burning in eastern China. J. Geophys. Res. Atmos. 118, 7389–7399.

Di Lorenzo, R.A., Young, C.J., 2016. Size separation method for absorption characterization in brown carbon: application to an aged biomass burning sample. Geophys. Res. Lett. 43, 458–465.

Du, Z., He, K., Cheng, Y., Duan, F., Ma, Y., Liu, J., Zhang, X., Zheng, M., Weber, R., 2014. A yearlong study of water-soluble organic carbon in Beijing II: light absorption properties. Atmos. Environ. 89, 235–241.

Du, A., Li, Y., Sun, J., Zhang, Z., You, B., Li, Z., Chen, C., Li, J., Qiu, Y., Liu, X., Ji, D., Zhang, W., Xu, W., Fu, P., Sun, Y., 2022. Rapid transition of aerosol optical properties and water-soluble organic aerosols in cold season in Fenwei Plain. Sci. Total Environ. 829, 154661.

Ervens, B., Feingold, G., Kreidenweis, S.M., 2005. Influence of water-soluble organic carbon on cloud drop number concentration. J. Geophys. Res.-Atmos. 110.

Fountoukis, C., Nenes, A., 2007. ISORROPIA II: a computationally efficient thermodynamic equilibrium model for K + -Ca2 + -Mg2 + -NH4 + -Na + -SO42–NO3–Cl–H2O aerosols. Atmos. Chem. Phys. 7, 4639–4659.

Frka, S., Sala, M., Kroflic, A., Hus, M., Cusak, A., Grgic, I., 2016. Quantum chemical calculations resolved identification of methylnitrocatechols in atmospheric aerosols. Environ. Sci. Technol. 50, 5526–5535.

Gao, Y., Zhang, Y., 2018. Formation and photochemical properties of aqueous brown carbon through glyoxal reactions with glycine. RSC Adv. 8, 38566–38573.

Ge, X., Li, L., Chen, Y., Chen, H., Wu, D., Wang, J., Xie, X., Ge, S., Ye, Z., Xu, J., Chen, M., 2017. Aerosol characteristics and sources in Yangzhou, China resolved by offline aerosol mass spectrometry and other techniques. Environ. Pollut. 225, 74–85.

Gilardoni, S., Massoli, P., Paglione, M., Giulianelli, L., Carbone, C., Rinaldi, M., Decesari, S., Sandrini, S., Costabile, F., Gobbi, G.P., Pietrogrande, M.C., Visentin, M., Scotto, F., Fuzzi, S., Facchini, M.C., 2016. Direct observation of aqueous secondary organic aerosol from biomass-burning emissions. Proc. Natl. Acad. Sci. 113, 10013.

Graber, E.R., Rudich, Y., 2006. Atmospheric HULIS: how humic-like are they? A comprehensive and critical review. Atmos. Chem. Phys. 6, 729–753.

Guo, H., Xu, L., Bougiatioti, A., Cerully, K.M., Capps, S.L., Hite Jr., J.R., Carlton, A.G., Lee, S.H., Bergin, M.H., Ng, N.L., Nenes, A., Weber, R.J., 2015. Fine-particle water and pH in the southeastern United States. Atmos. Chem. Phys. 15, 5211–5228.

Haynes, J.P., Miller, K.E., Majestic, B.J., 2019. Investigation into photoinduced auto-oxidation of polycyclic aromatic hydrocarbons resulting in brown carbon production. Environ. Sci. Technol. 53, 682–691.

Hecobian, A., Zhang, X., Zheng, M., Frank, N., Edgerton, E.S., Weber, R.J., 2010. Water-soluble organic aerosol material and the light-absorption characteristics of aqueous extracts measured over the Southeastern United States. Atmos. Chem. Phys. 10, 5965–5977.

Hems, R.F., Abbatt, J.P.D., 2018. Aqueous phase photo-oxidation of brown carbon nitrophenols: reaction kinetics, mechanism, and evolution of light absorption. ACS Earth Space Chem. 2, 225–234.

Hems, R.F., Schnitzler, E.G., Bastawrous, M., Soong, R., Simpson, A.J., Abbatt, J.P.D., 2020. Aqueous photoreactions of wood smoke brown carbon. ACS Earth Space Chem. 4, 1149–1160.

Hems, R.F., Schnitzler, E.G., Liu-Kang, C., Cappa, C.D., Abbatt, J.P.D., 2021. Aging of atmospheric brown carbon aerosol. ACS Earth Space Chem. 5, 722–748.
Hennigan, C.J., Izumi, J., Sullivan, A.P., Weber, R.J., Nenes, A., 2015. A critical evaluation of proxy methods used to estimate the acidity of atmospheric particles. Atmos. Chem. Phys. 15, 2775–2790.
Herrmann, H., Schaefer, T., Tilgner, A., Styler, S.A., Weller, C., Teich, M., Otto, T., 2015. Tropospheric aqueous-phase chemistry: kinetics, mechanisms, and its coupling to a changing gas phase. Chem. Rev. 115, 4259–4334.
Hu, Z., Kang, S., Li, C., Yan, F., Chen, P., Gao, S., Wang, Z., Zhang, Y., Sillanpää, M., 2017. Light absorption of biomass burning and vehicle emission-sourced carbonaceous aerosols of the Tibetan Plateau. Environ. Sci. Pollut. Res. 24, 15369–15378.
Huang, R.-J., Zhang, Y., Bozzetti, C., Ho, K.-F., Cao, J.-J., Han, Y., Daellenbach, K.R., Slowik, J.G., Platt, S.M., Canonaco, F., Zotter, P., Wolf, R., Pieber, S.M., Bruns, E.A., Crippa, M., Ciarelli, G., Piazzalunga, A., Schwikowski, M., Abbaszade, G., Schnelle-Kreis, J., Zimmermann, R., An, Z., Szidat, S., Baltensperger, U., Haddad, I.E., Prévôt, A.S.H., 2014. High secondary aerosol contribution to particulate pollution during haze events in China. Nature 514, 218–222.
Jiang, X., Liu, D., Li, Q., Tian, P., Wu, Y., Li, S., Hu, K., Ding, S., Bi, K., Li, R., Huang, M., Ding, D., Chen, Q., Kong, S., Li, W., Pang, Y., He, D., 2022. Connecting the light absorption of atmospheric organic aerosols with oxidation state and polarity. Environ. Sci. Technol. 56, 12873–12885.
Kasthuriarachchi, N.Y., Rivellini, L.-H., Chen, X., Li, Y.J., Lee, A.K.Y., 2020. Effect of relative humidity on secondary brown carbon formation in aqueous droplets. Environ. Sci. Technol. 54, 13207–13216.
Kim, H., Kim, J.Y., Jin, H.C., Lee, J.Y., Lee, S.P., 2016. Seasonal variations in the light-absorbing properties of water-soluble and insoluble organic aerosols in Seoul,Korea. Atmos. Environ. 129, 234–242.
Kim, H., Collier, S., Ge, X., Xu, J., Sun, Y., Jiang, W., Wang, Y., Herckes, P., Zhang, Q., 2019. Chemical processing of water-soluble species and formation of secondary organic aerosol in fogs. Atmos. Environ. 200, 158–166.
Kitanovski, Z., Čusak, A., Grgić, I., Claeys, M., 2014. Chemical characterization of the main products formed through aqueous-phase photonitration of guaiacol. Atmos. Chem. Phys. 7, 2457–2470.
Lambe, A.T., Cappa, C.D., Massoli, P., Onasch, T.B., Forestieri, S.D., Martin, A.T., Cummings, M.J., Croasdale, D.R., Brune, W.H., Worsnop, D.R., 2013. Relationship between oxidation level and optical properties of secondary organic aerosol. Environ. Sci. Technol. 47, 6349–6357.
Laskin, A., Laskin, J., Nizkorodov, S.A., 2015. Chemistry of atmospheric brown carbon. Chem. Rev. 115, 4335–4382.
Lee, H.J., Aiona, P.K., Laskin, A., Laskin, J., Nizkorodov, S.A., 2014. Effect of solar radiation on the optical properties and molecular composition of Llboratory proxies of atmospheric brown carbon. Environ. Sci. Technol. 48, 10217–10226.
Lei, Y., Shen, Z., Zhang, T., Zhang, Q., Wang, Q., Sun, J., Gong, X., Cao, J., Xu, H., Liu, S., Yang, L., 2018a. Optical source profiles of brown carbon in size-resolved particulate matter from typical domestic biofuel burning over Guanzhong Plain,China. Sci. Total Environ. 622–623, 244–251.
Lei, Y., Shen, Z., Wang, Q., Zhang, T., Cao, J., Sun, J., Zhang, Q., Wang, L., Xu, H., Tian, J., Wu, J., 2018b. Optical characteristics and source apportionment of brown carbon in winter PM2.5 over Yulin in Northern China. Atmos. Res. 213, 27–33.
Lei, Y., Shen, Z., Zhang, T., Lu, D., Zeng, Y., Zhang, Q., Xu, H., Bei, N., Wang, X., Cao, J., 2019. High time resolution observation of PM2.5 brown carbon over Xi'an in northwestern China: seasonal variation and source apportionment. Chemosphere 237, 124530.
Lei, Y., Shen, Z., He, K., Li, L., Qin, Y., Zeng, Y., Li, J., Xu, H., Ma, Y., Zhang, T., Yang, L., Zhang, N., Cao, J., 2021. The formation and evolution of parent and oxygenated polycyclic aromatic hydrocarbons during a severe winter haze–fog event over Xi'an,China. Environ. Sci. Pollut. Res. 28, 9165–9172.
Lei, Y., Wang, Z., Xu, H., Feng, R., Zhang, N., Zhang, Y., Du, W., Zhang, Q., Wang, Q., Li, L., Qu, L., Hang Ho, S.S., Shen, Z., Cao, J., 2022. Characteristics and health risks of parent, alkylated, and oxygenated PAHs and their contributions to reactive oxygen species from PM2.5 vehicular emissions in the longest tunnel in downtown Xi'an, China. Environ. Res. 212, 113357.
Li, J., Wang, G., Ren, Y., Wang, J., Wu, C., Han, Y., Zhang, L., Cheng, C., Meng, J., 2016. Identification of chemical compositions and sources of atmospheric aerosols in Xi'an, inland China during two types of haze events. Sci. Total Environ. 566–567, 230–237.
Li, J., Zhang, Q., Wang, G., Li, J., Wu, C., Liu, L., Wang, J., Jiang, W., Li, L., Ho, K.F., Cao, J., 2020a. Optical properties and molecular compositions of water-soluble and water-insoluble brown carbon (BrC) aerosols in northwest China. Atmos. Chem. Phys. 20, 4889–4904.
Li, J., Chen, Q., Hua, X., Chang, T., Wang, Y., 2020b. Occurrence and sources of chromophoric organic carbon in fine particulate matter over Xi'an, China. Sci. Total Environ. 725, 138290.
Li, X., Zhao, Q., Yang, Y., Zhao, Z., Liu, Z., Wen, T., Hu, B., Wang, Y., Wang, L., Wang, G., 2021a. Composition and sources of brown carbon aerosols in megacity Beijing during the winter of 2016. Atmos. Res. 262, 105773.
Li, D., Zhao, Y., Du, W., Zhang, Y., Chen, Y., Lei, Y., Wu, C., Wang, G., 2022. Characterization of PM2.5-bound parent and oxygenated PAHs in three cities under the implementation of clean air action in northern China. Atmos. Res. 267, 105932.
Li, D., Wu, C., Zhang, S., Lei, Y., Lv, S., Du, W., Liu, S., Zhang, F., Liu, X., Liu, L., Meng, J., Wang, Y., Gao, J., Wang, G., 2023. Significant coal combustion contribution to water-soluble brown carbon during winter in Xingtai, China: optical properties and sources. J. Environ. Sci. 124, 892–900.
Lin, P., Engling, G., Yu, J.Z., 2010. Humic-like substances in fresh emissions of rice straw burning and in ambient aerosols in the Pearl River Delta Region, China. Atmos. Chem. Phys. 10, 6487–6500.
Liu, J., Bergin, M., Guo, H., King, L., Kotra, N., Edgerton, E., Weber, R.J., 2013. Size-resolved measurements of brown carbon in water and methanol extracts and estimates of their contribution to ambient fine particle light absorption. Atmos. Chem. Phys. 13, 12389.
Liu, M., Song, Y., Zhou, T., Xu, Z., Yan, C., Zheng, M., Wu, Z., Hu, M., Wu, Y., Zhu, T., 2017. Fine particle pH during severe haze episodes in northern China. Geophys. Res. Lett. 44, 5213–5221.
Liu, Y., Lu, J., Chen, Y., Liu, Y., Ye, Z., Ge, X., 2020. Aqueous-phase production of secondary organic aerosols from oxidation of dibenzothiophene (DBT). Atmosphere 11, 151.
Lu, J., Ge, X., Liu, Y., Chen, Y., Xie, X., Ou, Y., Ye, Z., Chen, M., 2019. Significant secondary organic aerosol production from aqueous-phase processing of two intermediate volatility organic compounds. Atmos. Environ. 211, 63–68.
Lv, S., Wang, F., Wu, C., Chen, Y., Liu, S., Zhang, S., Li, D., Du, W., Zhang, F., Wang, H., Huang, C., Fu, Q., Duan, Y., Wang, G., 2022. Gas-to-aerosol phase partitioning of atmospheric water-soluble organic compounds at a rural site in China: an enhancing effect of NH3 on SOA formation. Environ. Sci. Technol. 56, 3915–3924.
Moschos, V., Kumar, N.K., Daellenbach, K.R., Baltensperger, U., Prévôt, A.S.H., El Haddad, I., 2018. Source apportionment of brown carbon absorption by coupling ultraviolet–visible spectroscopy with aerosol mass spectrometry. Environ. Sci. Technol. Lett. 5, 302–308.
Qin, Y., Tan, H., Li, Y.J., Li, Z., Schurman, M.I., Liu, L., Wu, C., Chan, C.K., 2018. Chemical characteristics of brown carbon in atmospheric particles at a suburban site near Guangzhou, China. Atmos. Chem. Phys. 18, 16409–16418.
Qiu, Y., Xie, Q., Wang, J., Xu, W., Li, L., Wang, Q., Zhao, J., Chen, Y., Chen, Y., Wu, Y., Du, W., Zhou, W., Lee, J., Zhao, C., Ge, X., Fu, P., Wang, Z., Worsnop, D.R., Sun, Y., 2019. Vertical characterization and source apportionment of water-soluble organic aerosol with High – resolution Aerosol Mass Spectrometry in Beijing, China. ACS Earth Space Chem. 3, 273–284.
Rodriguez, A.A., Rafla, M.A., Welsh, H.G., Pennington, E.A., Casar, J.R., Hawkins, L.N., Jimenez, N.G., de Loera, A., Stewart, D.R., Rojas, A., Tran, M.-K., Lin, P., Laskin, A., Formenti, P., Cazaunau, M., Pangui, E., Doussin, J.-F., De Haan, D.O., 2022. Kinetics, products, and brown carbon formation by aqueous-phase reactions of glycolaldehyde with atmospheric amines and ammonium sulfate. J. Phys. Chem. A 126, 5375–5385.
de Sá, S.S., Rizzo, L.V., Palm, B.B., Campuzano-Jost, P., Day, D.A., Yee, L.D., Wernis, R., Isaacman-VanWertz, G., Brito, J., Carbone, S., Liu, Y.J., Sedlacek, A., Springston, S., Goldstein, A.H., Barbosa, H.M.J., Alexander, M.L., Artaxo, P., Jimenez, J.L., Martin, S.T., 2019. Contributions of biomass-burning, urban, and biogenic emissions to the concentrations and light-absorbing properties of particulate matter in central Amazonia during the dry season. Atmos. Chem. Phys. 19, 7973–8001.
Shen, Z., Zhang, Q., Cao, J., Zhang, L., Lei, Y., Huang, Y., Huang, R.J., Gao, J., Zhao, Z., Zhu, C., Yin, X., Zheng, C., Xu, H., Liu, S., 2017. Optical properties and possible sources of brown carbon in PM2.5 over Xi'an, China. Atmos. Environ. 150, 322–330.
Srinivas, B., Sarin, M.M., 2014. Brown carbon in atmospheric outflow from the Indo-Gangetic Plain: mass absorption efficiency and temporal variability. Atmos. Environ. 89, 835–843.
Sumlin, B.J., Pandey, A., Walker, M.J., Pattison, R.S., Williams, B.J., Chakrabarty, R.K., 2017. Atmospheric photooxidation diminishes light absorption by primary brown carbon aerosol from biomass burning. Environ. Sci. Technol. Lett. 4, 540–545.
Sun, Y., Zhang, Q., Zheng, M., Ding, X., Edgerton, E.S., Wang, X., 2011. Characterization and source apportionment of water-soluble organic matter in atmospheric fine particles (PM2.5) with high-resolution aerosol mass spectrometry and GC–MS. Environ. Sci. Technol. 45, 4854–4861.
Twohy, C.H., Anderson, J.R., Crozier, P.A., 2005. Nitrogenated organic aerosols as cloud condensation nuclei. Geophys. Res. Lett. 32.
Wang, G., Wang, H., Yu, Y., Gao, S., Feng, J., Gao, S., Wang, L., 2003. Chemical characterization of water-soluble components of PM10 and PM2.5 atmospheric aerosols in five locations of Nanjing, China. Atmos. Environ. 37, 2893–2902.
Wang, G., Kawamura, K., Xie, M., Hu, S., Gao, S., Cao, J., An, Z., Wang, Z., 2009. Size-distributions of n-alkanes, PAHs and hopanes and their sources in the urban, mountain and marine atmospheres over East Asia. Atmos. Chem. Phys. 9, 8869–8882.
Wang, G., Zhang, R., Gomez, M.E., Yang, L., Levy Zamora, M., Hu, M., Lin, Y., Peng, J., Guo, S., Meng, J., Li, J., Cheng, C., Hu, T., Ren, Y., Wang, Y., Gao, J., Cao, J., An, Z., Zhou, W., Li, G., Wang, J., Tian, P., Marrero-Ortiz, W., Secrest, J., Du, Z., Zheng, J., Shang, D., Zeng, L., Shao, M., Wang, W., Huang, Y., Wang, Y., Zhu, Y., Li, Y., Hu, J., Pan, B., Cai, L., Cheng, Y., Ji, Y., Zhang, F., Rosenfeld, D., Liss, P.S., Duce, R.A., Kolb, C.E., Molina, M.J., 2016a. Persistent sulfate formation from London fog to Chinese haze. Proc. Natl. Acad. Sci. 113, 13630–13635.
Wang, X., Heald, C.L., Sedlacek, A.J., de Sá, S.S., Martin, S.T., Alexander, M.L., Watson, T.B., Aiken, A.C., Springston, S.R., Artaxo, P., 2016b. Deriving brown carbon from multiwavelength absorption measurements: method and application to AERONET and Aethalometer observations. Atmos. Chem. Phys. 16, 12733–12752.
Wang, G., Zhang, F., Peng, J., Duan, L., Ji, Y., Marrero-Ortiz, W., Wang, J., Li, J., Wu, C., Cao, C., Wang, Y., Zheng, J., Secrest, J., Li, Y., Wang, Y., Li, H., Li, N., Zhang, R., 2018a. Particle acidity and sulfate production during severe haze events in China cannot be reliably inferred by assuming a mixture of inorganic salts. Atmos. Chem. Phys. 18, 10123–10132.
Wang, X., Heald, C.L., Liu, J., Weber, R.J., Campuzano-Jost, P., Jimenez, J.L., Schwarz, J.P., Perring, A.E., 2018b. Exploring the observational constraints on the simulation of brown carbon. Atmos. Chem. Phys. 18, 635–653.
Wang, Q., Ye, J., Wang, Y., Zhang, T., Ran, W., Wu, Y., Tian, J., Li, L., Zhou, Y., Hang Ho, S.S., Dang, B., Zhang, Q., Zhang, R., Chen, Y., Zhu, C., Cao, J., 2019. Wintertime optical properties of primary and secondary brown carbon at a regional site in the North China Plain. Environ. Sci. Technol. 53, 12389–12397.
Wang, J., Ye, J., Zhang, Q., Zhao, J., Wu, Y., Li, J., Liu, D., Li, W., Zhang, Y., Wu, C., Xie, C., Qin, Y., Lei, Y., Huang, X., Guo, J., Liu, P., Fu, P., Li, Y., Lee, H.C., Choi, H., Zhang, J., Liao, H., Chen, M., Sun, Y., Ge, X., Martin, S.T., Jacob, D.J., 2021. Aqueous production of secondary organic aerosol from fossil-fuel emissions in winter Beijing haze. Proc. Natl. Acad. Sci. 118, e2022179118.
Wang, D., Shen, Z., Zhang, Q., Lei, Y., Zhang, T., Huang, S., Sun, J., Xu, H., Cao, J., 2022. Winter brown carbon over six of China's megacities: light absorption, molecular characterization, and improved source apportionment revealed by multilayer perceptron neural network. Atmos. Chem. Phys. 22, 14893–14904.
Wong, J.P.S., Nenes, A., Weber, R.J., 2017. Changes in light absorptivity of molecular weight separated brown carbon due to photolytic aging. Environ. Sci. Technol. 51, 8414–8421.

Wong, J.P.S., Tsagkaraki, M., Tsiodra, I., Mihalopoulos, N., Violaki, K., Kanakidou, M., Sciare, J., Nenes, A., Weber, R.J., 2019. Atmospheric evolution of molecular-weight-separated brown carbon from biomass burning. Atmos. Chem. Phys. 19, 7319–7334.

Wu, C., Wang, G., Cao, C., Li, J., Li, J., Wu, F., Huang, R., Cao, J., Han, Y., Ge, S., Xie, Y., Xue, G., Wang, X., 2019. Chemical characteristics of airborne particles in Xi'an, inland China during dust storm episodes: implications for heterogeneous formation of ammonium nitrate and enhancement of N−deposition. Environ. Pollut. 244, 877–884.

Wu, C., Wang, G., Li, J., Li, J., Cao, C., Ge, S., Xie, Y., Chen, J., Li, X., Xue, G., Wang, X., Zhao, Z., Cao, F., 2020. The characteristics of atmospheric brown carbon in Xi'an, inland China: sources, size distributions and optical properties. Atmos. Chem. Phys. 20, 2017–2030.

Xie, M., Chen, X., Holder, A.L., Hays, M.D., Lewandowski, M., Offenberg, J.H., Kleindienst, T.E., Jaoui, M., Hannigan, M.P., 2019. Light absorption of organic carbon and its sources at a southeastern U.S. location in summer. Environ. Pollut. 244, 38–46.

Xu, H., Feng, R., Wang, Z., Zhang, N., Zhang, R., He, K., Wang, Q., Zhang, Q., Sun, J., Zhang, B., Shen, Z., Ho, S.H.S., Cao, J., 2021. Environmental and health risks of VOCs in the longest inner–city tunnel in Xi'an, Northwest China: implication of impact from new energy vehicles. Environ. Pollut. 282, 117057.

Ye, Z., Liu, J., Gu, A., Feng, F., Liu, Y., Bi, C., Xu, J., Li, L., Chen, H., Chen, Y., Dai, L., Zhou, Q., Ge, X., 2017. Chemical characterization of fine particulate matter in Changzhou, China, and source apportionment with offline aerosol mass spectrometry. Atmos. Chem. Phys. 17, 2573–2592.

Yu, L., Smith, J., Laskin, A., Anastasio, C., Zhang, Q., 2014. Chemical characterization of SOA formed from aqueous-phase reactions of phenols with the triplet excited state of carbonyl and hydroxyl radical. Atmos. Chem. Phys. 2014, 21149–21187.

Zeng, Y., Ning, Y., Shen, Z., Zhang, L., Zhang, T., Lei, Y., Zhang, Q., Li, G., Xu, H., Ho, S.S.H., Cao, J., 2021. The roles of N, S, and O in molecular absorption features of brown carbon in PM2.5 in a typical semi-arid megacity in Northwestern China. J. Geophys. Res. Atmos. 126, e2021JD034791.

Zhang, R., Wang, G., Guo, S., Zamora, M.L., Ying, Q., Lin, Y., Wang, W., Hu, M., Wang, Y., 2015. Formation of urban fine particulate matter. Chem. Rev. 115, 3803–3855.

Zhang, Q., Shen, Z., Zhang, L., Zeng, Y., Ning, Z., Zhang, T., Lei, Y., Wang, Q., Li, G., Sun, J., Westerdahl, D., Xu, H., Cao, J., 2020. Investigation of primary and secondary particulate brown carbon in two Chinese cities of Xi'an and Hong Kong in wintertime. Environ. Sci. Technol. 54, 3803–3813.